The hysteretic response of a shallow pyroclastic deposit

Luca Comegna[1], Emilia Damiano[1], Roberto Greco[1], Lucio Olivares[1], Luciano Picarelli[2]

[1]Department of Engineering, University of Campania "Luigi Vanvitelli", Aversa, 81031, Italy
[2]JTC1 "Natural Slopes and Landslides", Chair, Federation of International Geo-Engineering Societies (FedIGS), Naples, 80131, Italy

Correspondence to: Luca Comegna (luca.comegna@unicampania.it)

Abstract. In the last decades, in Campania (Southern Italy), steep slopes mantled by loose air-fall pyroclastic soils have been the seat of shallow fast rainfall-induced landslides. The occurrence of such events has been the result of the combination of critical rainstorms and of unfavourable initial conditions determined by antecedent infiltration/evaporation/drainage processes.

In order to understand the nature of the phenomena at hand and to clarify the role of all influencing factors, an automatic monitoring station has been installed in an area already subject to a recent killer flowslide (December, 1999). The paper reports ~~field~~ data collected in 2011 about volumetric water content and suction (used to investigate the soil water retention features) and rainfall depth and temperature (providing the boundary conditions). ~~provided by the automatic monitoring of the annual hydrological response of a shallow deposit of loose pyroclastic soils located in a mountainous area of Campania, Southern Italy. The monitoring station is installed along the northern slope of mount Cornito, about 2 km east of the town of Cervinara, which in December 1999 had been involved in a rainfall induced flowslide. The collected data concern rainfall height, soil moisture content and suction.~~ In particular, the installation at the same depths of tensiometers and Time Domain Reflectometry (TDR) ~~suction and moisture~~ sensors ~~allows~~ allowed ~~to estimate the soil water retention features that seem~~ to ~~indicate~~ recognize ~~some~~ the hysteretic nature of the wetting/drying ~~processes~~ soil response ~~induced~~ to ~~by~~ weather ~~conditions~~forcing and ~~their~~ its influence on the ~~local~~ slope stability conditions.

The data reported in the paper are freely available at https://doi.org/10.5281/zenodo.4281166 (Comegna et al., 2020).

1 Introduction

The hydraulic response of unsaturated soils subjected to infiltration and/or evaporation phenomena is usually modelled through the well-known *Soil Water Retention Curve*, SWRC, correlating matric suction, s, with volumetric water content, θ. Experimental evidence and theoretical considerations (e.g., Mualem, 1976; Pham, 2002; Wheeler et al., 2003; Tami et al., 2004; Li, 2005; Tarantino, 2009; Yang et al., 2012; Pirone et al., 2014; Comegna et al., 2016c; Chen et al., 2017; Chen et al., 2019; Rianna et al., 2019) indicate that the SWRC is not univocal, but may depend on soil initial conditions and on the induced wetting or drying paths~~, revealing an hysteretic nature~~. This soil response, known as *hydraulic hysteresis*, may be related to microscopic phenomena affecting the energy state of water at pore scale (i.e. variations of contact angle during

solid particles wetting and drying, or bottlenecks differently affecting filling and emptying of pores), as well as macroscopic phenomena depending on the boundary conditions and on the rate of the specific transient wetting/drying process (e.g. air entrapment). Figure 1 shows the typical response of an initially saturated soil ~~specimen~~ sample subjected to drying and wetting cycles. During the first drying stage, ~~the volumetric water content~~ θ decreases from the initial value, $\theta_{s,d}$, following a path, known as the *main drying curve*, until attaining the minimum, corresponding to a high ~~suction~~ s value, known as the "residual ~~soil moisture~~volumetric water content", θ_r. In the subsequent wetting process ~~the volumetric water content~~ θ increases along a different path, known as the *main wetting curve* (Fig. 1), until reaching a final maximum value, $\theta_{s,w}$, at ~~zero suction~~ $s = 0$: $\theta_{s,w}$ is usually different from $\theta_{s,d}$ because of some air entrapment that does not allow full soil~~prevents to reach a~~ saturation ~~degree equal to one~~. However, in some cases, if the wetting process is very slow, it may occur that $\theta_{s,w} \cong \theta_{s,d}$.

If ~~moving along~~ a reverse process takes place along one of these paths ~~a reverse process is initiated~~, the main path is abandoned and a different *scanning curve*, located between the two main paths, is then travelled (Fig. 1). Scanning curves, which in turn may be characterised by internal hysteretic loops, present a lower slope than the main curves: this physically means that, starting from the same ~~matric suction~~ s value, the θ variation ~~in soil moisture~~ corresponding to a given ~~suction~~ s change is smaller running a scanning than a main curve. As shown in Figure 1, the final part of a scanning path may coincide with the nearest primary curve. ~~Concerning this point,~~ This result has been experimentally recognized by Tami et al. (2004) ~~report the results of~~ through some tests carried out on a 30° model slope consisting of a 40 cm thick layer of fine sands, overlying a 20 cm thick layer of gravelly sands, subjected to artificial precipitation~~s~~ of different intensity. Figure 2a shows the scanning curves obtained by fitting the coupled data measured by a tensiometer and a Time Domain Reflectometry (TDR) probe located at a depth of 30 cm (Fig. 2b) during two consecutive drying stages (1-2, 2-3) and two consecutive wetting stages (4-5, 5-6). The main drying and wetting curves had been independently obtained through a Tempe cell and capillary rise tests. Therefore, the same θ may be associated with different water potential energies, thus with different s values within an interval defined by the highest and lowest limits respectively imposed by the main drying curve and the main wetting curve.

Even though often observed in laboratory experiments, the hydraulic hysteretic response of unsaturated soils is still often neglected at slope scale, being usually modelled by a single Soil Water Retention Curve fitting all the available experimental data. This choice is frequently due to unavailability of detailed field information. Most of the knowledge is in fact based on the results of laboratory investigations and/or of physical modelling. These tests, although very useful, are unavoidably not able to take into account further aspects that that could make the actual hysteretic response of natural slopes quite different from what is observed in the lab, as the influence of different boundary conditions, the role of root water uptake or of the atmospheric evaporative demand, etc.

Considering that the hydrological response could affect the stability conditions of natural slopes, an automatic monitoring station was installed in a shallow layer of loose pyroclastic soils covering a steep mountainous area in a site of Campania Region (Southern Italy), which in 1999 was the seat of a rainfall-induced flowslide (Damiano et al., 2012). The availability

of continuous data, consisting of rainfall depth, temperature, volumetric water content and suction readings, allowed to collect useful information from January, 2011, to January, 2012, that have been also used to estimate the slope stability conditions at the investigated depths.

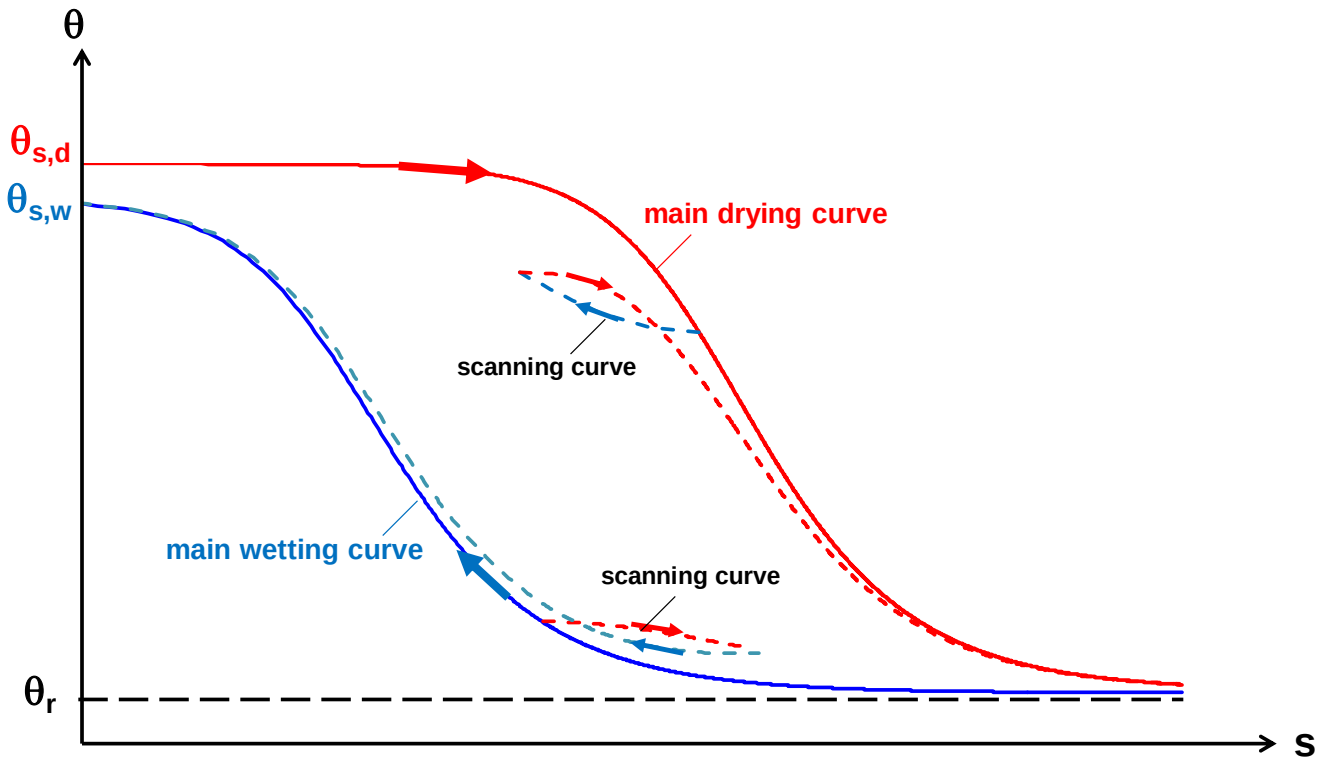

Figure 1: Hysteretic wetting/drying paths.

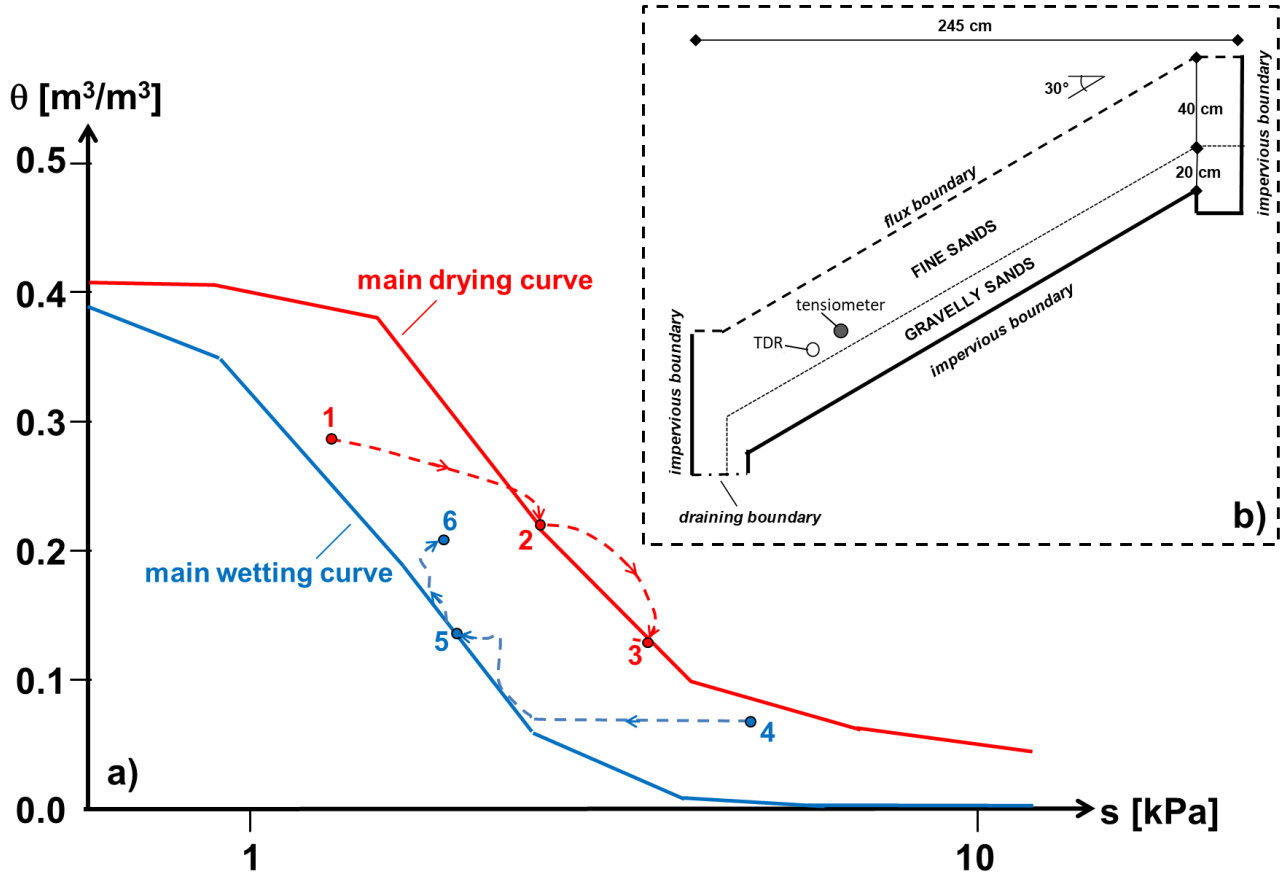

Figure 2: Scanning curves obtained from flume tests carried out by Tami et al. (2004).

75

~~The described hydraulic soil response, known as *hydraulic hysteresis*, may be related to microscopic phenomena affecting the energy state of water at pore scale (i.e. variations of contact angle during solid particles wetting and drying, or bottlenecks differently affecting filling and emptying of pores), as well as macroscopic phenomena depending on the boundary conditions and on the rate of the specific transient wetting/drying process (e.g. air entrapment).~~

80 ~~Consequently, the same water content may be associated with different water potential energies, thus with different suction values within an interval defined by the highest and lowest limits respectively imposed by the main drying curve and the main wetting curve.~~

~~Field monitoring is doubtless a helpful tool to fully understand the hydrological behaviour of soils. Well aware that such response could in turn affect the stability conditions of the slope, an automatic monitoring station has been installed in a~~

85 ~~shallow layer of loose pyroclastic soils covering a steep mountainous area in a site in Campania Region (Southern Italy), which in 1999 had been the seat of rainfall induced flowslide causing the death of four people (Olivares and Picarelli, 2003). The availability of continuous data, consisting of rainfall height, soil moisture content and suction readings, allowed to~~

~~collect useful information. The data reported in the present paper concern the time period going from January, 2011, to January, 2012. Such data have been also used to estimate the slope stability conditions at the investigated depths.~~

2 Data and methods

2.1 ~~Monitoring site~~ Geomorphological and climate framework

The investigated site is located at an elevation of 560 m a.s.l., on the North-East facing slope of mount Cornito (Fig. 3a), 2 km ~~far~~ from the town of Cervinara (Campania Region, Southern Italy), about 50 km northeast of Naples. On December, 16th, 1999, the slope was involved in a disastrous flowslide induced by a rainstorm of 320 mm in 50 hours. The landslide body entered the narrow Cornito stream reaching the about 2.5 km downslope town (Fig. 3b), where it caused heavy damage and five victims.~~ The area is characterised by a humid Mediterranean climate, with most precipitations occurring between October and April and warm and dry summer. The mean annual rainfall height is around 1600 mm, and the mean annual potential evapotranspiration around 750 mm (Marino et al., 2020). Figure 4 reports mean monthly values of rainfall height, mean daily temperature and evapotranspiration.~~

Geological surveys and geotechnical investigations reveal that the basal Mesozoic–Cenozoic fractured limestones are overlain by air-fall sandy soils resulting from the explosive volcanic activity of Somma–Vesuvius and Phleagraean Fields (e.g., Fiorillo et al., 2001; ~~Picarelli et al., 2006;~~ Damiano et al., 2012). In particular, the pyroclastic deposits consist of alternating layers of ashes and pumices, more or less parallel to the bedrock surface, with a thickness strongly dependent on the slope angle, ranging from some decimetres in the steepest upslope zones (about 50°) to more than 10 m at the foot of the hill (Guadagno et al., 2011). In some verticals, ~~Some~~ some layers ~~locally miss~~were not found, possibly as a result of past landslides or of erosive processes.

Cultivated chestnut trees are widespread on the slope, except some areas where the vegetation consists of shrubs and grass. When the tree foliage is present, usually from May to late September, a dense underbrush grows, mainly formed by ferns and other seasonal shrubs. Differently, in October ~~the~~ leaves ~~get dry and~~ fall from the trees, and the underbrush disappears until the following late spring. During late autumn and winter the ground is mostly covered by a layer of litter, mainly originating from fallen chestnut leaves. The seasonal variations of vegetation affect the soil hydrologic response to meteorological forcing by: i) interception of the precipitation and ii) root water uptake (Comegna et al., 2013). Interception is caused by canopy, understory and litter~~:. ii) root water uptake, that distributes the~~ The total evapotranspiration flux, distributed over the root depth~~,~~ according to the local value of soil water potential, ~~which~~ is highly variable throughout the year owing to the dormant leafless vegetation in winter ~~(Comegna et al., 2013)~~. Visual inspections in trenches dug during the investigations that have been carried out on site showed that roots usually extend across the entire soil depth up the basal limestones, with a maximum density within the uppermost 0.50 m of soil cover, becoming sparse below the depth of 1.50 m.

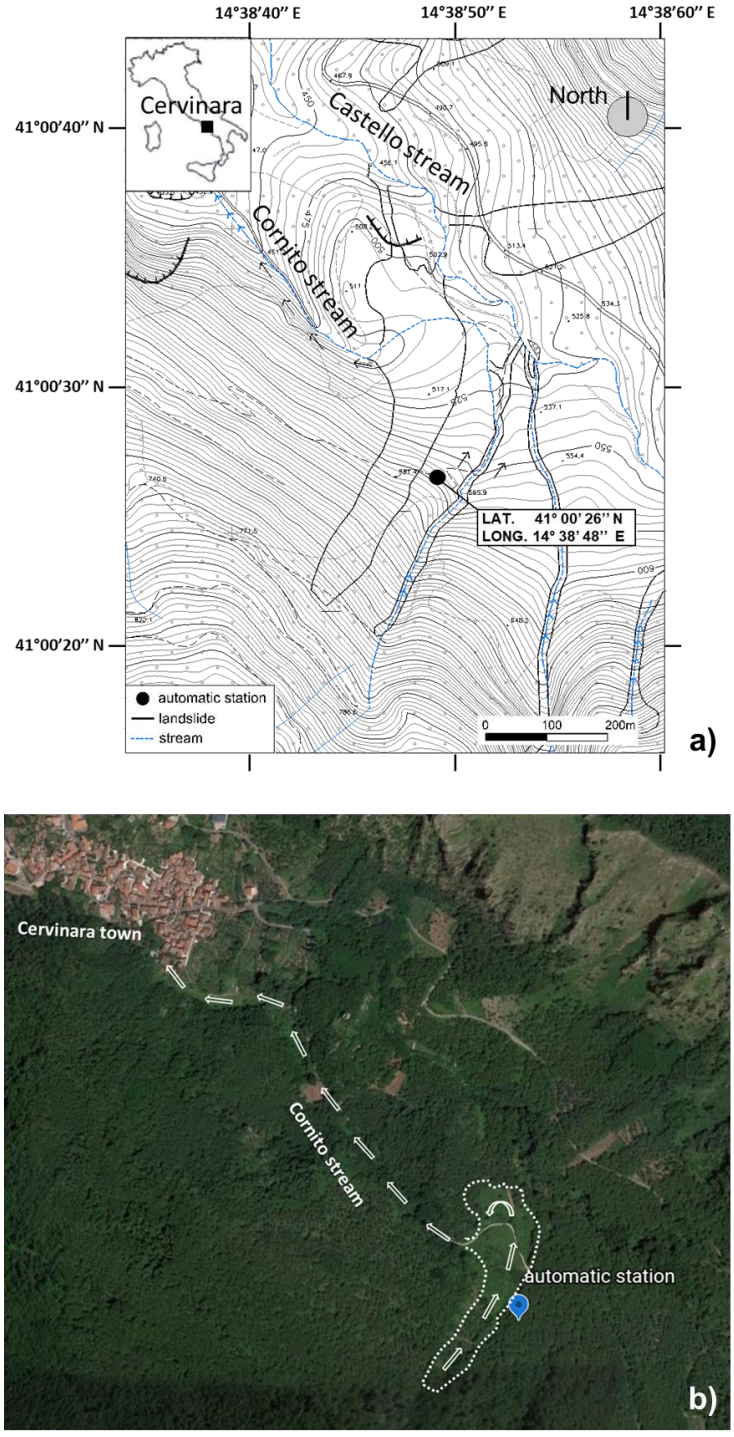

120

Figure 3: Location of the automatic monitoring station: ~~(modified after~~topographic map (provided by Damiano, 2004) (a), and ~~sketch of the local stratigraphy and position of the sensors~~aerial photo of the site provided by Google Earth (https://www.google.it/intl/it/earth/) (b).

Concerning climate, Figure 4 shows mean monthly values of rainfall depth calculated with the 2001-2017 data from the rain gauge installed in Cervinara, at the elevation of 320 m a.s.l., by the meteorological alert network managed by the "Functional Centre for forecast, prevention and monitoring of risks and alerting for civil protection" of Campania Civil Protection Agency. The mean annual rainfall depth is around 1600 mm: as typical of the Mediterranean climate, most precipitation occur between October and April, while summer is essentially dry. Figure 4 also reports mean monthly temperature calculated with the data monitored from 1979 to 1998 by the meteorological station of Montesarchio, managed by the National Hydrological Service, which is located 4 km from the test site and approximately at the same elevation. These data have been used for the estimation with the Thornthwaite expression (1946) of the monthly potential evapotranspiration, PET; in particular, the estimated PET annual value is around 750 mm (Marino et al., 2020).

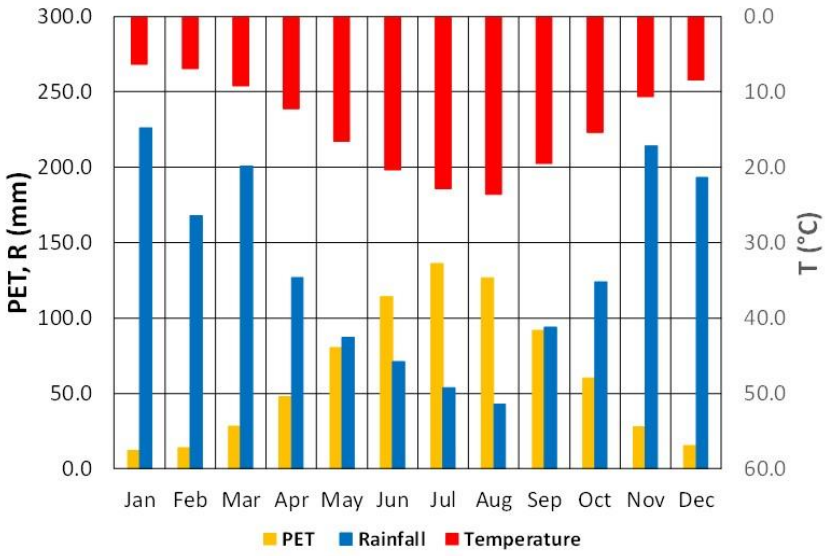

Figure 4: Mean monthly values of rainfall depth, R, temperature, T, and potential evapotranspiration, PET (estimated with the Thornthwaite expression, 1946).

2.2 Soil properties

~~The monitored deposit is 1.9 m thick with a sloping angle of about 40°.~~ Thanks to a number of field investigations and geotechnical laboratory tests (carried out both on undisturbed and reconstituted soil samples), Damiano et al. (2012) provide information about the physical and mechanical soil properties (Table 1). In the monitored verticals, the soil deposit is 1.9 m deep with a sloping angle of about 40° (Fig. 5). The local stratigraphy consists of the following unsaturated soil layers ~~(Fig. 3b)~~: 1) topsoil, 10 cm thick; 2) coarse pumices, 40 cm thick; 3) ashes, 1.30 m thick; 4) altered ashes, 10 cm thick, located just above the bedrock. The volcanic ash is a sandy silt, the pumices are sandy gravels. The lowermost ~~thin~~ altered ashes

~~layer~~ overlying the bedrock ~~is~~ are representative of a deteriorated thin ash layer, with a grain size which is turning from sandy silt to clayey and silty sand, featured by ~~with~~ a plasticity index ranging in the interval 10–30%. The soil porosity ranges between 50% and 75% ~~(Table 1)~~. The shear strength parameters are typical of essentially cohesionless coarse grains soils.

Table 1: Main physical and mechanical properties of the pyroclastic cover~~.~~: specific unit weight, γ_s; unit weight, γ; porosity; cohesion, c'; friction angle, φ'.

layer	γ_s [kN/m^3]	γ [kN/m^3]	porosity [%]	c'[kPa]	φ'[°]
coarse pumices	23	13	50-55	0	~~45~~
ashes	26	14	68-75	0	38
altered ashes	26	16	60	2	38

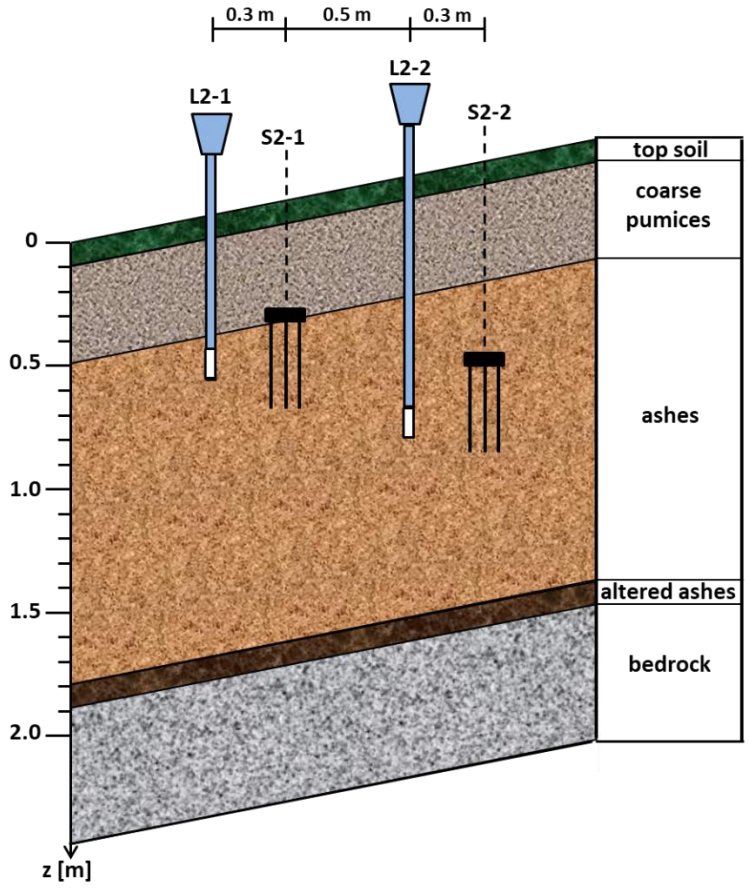

Figure 5: Local stratigraphy of the monitored deposit and position of the tensiometers (L2-1 and L2-2), and of the TDR sensors (S2-1, S2-2).

~~Monitoring started at the beginning of 2002 (Olivares et al., 2003; Damiano et al., 2012). Rainfall was automatically recorded at a hourly time step by a rain gauge having a sensitivity of 0.2 mm. Soil suction was manually measured by "Jet-fill" tensiometers equipped with a Bourdon manometer, installed at different depths in the ash layers. An additional automatic monitoring station has been installed in 2009. It consists of eight "Jet-fill" tensiometer, equipped with tension transducers, and of seven metallic probes for Time Domain Reflectometry (TDR) aimed at measuring volumetric water content (Comegna et al. 2016a). The ceramic tips of the tensiometerswere pushed into the soil through small holes previously dug by a drill. The uppermost part of the hole was then filled with a bentonite–cement mixture to avoid any water infiltration. A careful maintenance was granted by regularly checking the complete saturation of the instruments (especially after long-lasting dry periods) and filling the tube with de-aired water in order to remove air bubbles; moreover, the instruments were carefully checked after cold periods when low temperatures could freeze. The soil moisture sensors consist of three 100-400 mm long metallic rods having a diameter of 3 mm and spacing of 15 mm. Once vertically buried in the soil, the probes were connected through coaxial cables and a multiplexer to a Campbell Scientific Inc. TDR 100 reflectometer. TDR readings provide the soil bulk dielectric permittivity, ε_a, which can be converted to soil volumetric water content, θ, through a calibration relationship (Topp et al., 1980). A specific relationship has been purposely found by Guida et al. (2012) through targeted laboratory tests on undisturbed samples taken nearby the monitoring station; the average error in the estimation of the volumetric water content is ±0.02 m^3/m^3. All the sensors are connected to the Campbell Data Logger. The monitoring station is powered by a solar panel with a 12V backup battery. The automatic acquisition and storage of data is set with a time resolution of six hours.~~

~~The following section describes the field data collected from January, 1st, 2011 to January, 31st, 2012 at the depths z = 0.60 m and z = 1.00 m, where the 7 cm long tensiometer ceramic tips, L2-1 and L2-2, are located in the ash layer in vicinity of the 40 cm long TDR probes S2-1 and S2-2 (Fig. 3b). For the sake of clarity, it has to be pointed out the sensors sample different soil volumes; this might lead to an imperfect matching of data.~~

Regarding the water retention properties, Figure ~~5~~ 6 shows the results of nine laboratory wetting tests performed by Damiano and Olivares (2010) ~~and by Olivares et al (2019)~~. ~~Such~~ These tests were carried out in the laboratory on a 40 cm thick model slope formed with ~~Cervinara ash and~~ volcanic ashes ~~with same grain size~~ taken from Cervinara and the nearby Monteforte Irpino sloping site. The model slope, ~~was~~ reconstituted at the maximum field porosity of 75% (Table 1), was subjected to artificial precipitation. ~~During artificial infiltration tests,~~The ~~soil matric suction~~ s and ~~moisture content~~ θ measurements were respectively ~~measured~~ provided by a miniaturised tensiometer and a TDR probe installed close to each other at depths from 1.5 to 8.5 cm. The initial ~~soil moisture and suction~~ s and θ values were respectively in the range 15-60 kPa and 0.21-0.34 m^3/m^3 ~~and 15-60 kPa~~ (Fig. ~~5~~6). Once infiltration started, ~~The~~ the ~~wetting curve~~experimental points of each test first ran rather a flat ~~wetting~~ path and then, for s smaller than 4 kPa, a ~~steeper~~ more inclined path until ~~attaining~~ full saturation. All

t~~T~~he ~~experimental~~ points located along the steeper paths ~~along such a steepest curve~~ were fitted with the van Genuchten equation (1980)

$$\vartheta = \vartheta_r + \frac{\vartheta_s - \vartheta_r}{[1+(\alpha s)^n]^m} \quad (1),$$

where ϑ_s is the saturated volumetric water content, ϑ_r is the residual volumetric water content, α, *n* and *m* are fitting parameters. ~~assuming~~ Assuming θ_s = 0.75 m^3/m^3 (that corresponds to the soil porosity), ~~and~~ θ_r = 0 (a value which is consistent with the coarse-grained nature of the soil), and $m = \frac{n-1}{n}$ (according to Mualem, 1976), Table 2 shows the best fitting ~~α,~~ α and *n* ~~and *m*~~ values. In order to help the interpretation of the in-situ hydrological response, the obtained curve ~~is reported in the next section, together with the monitored field data~~will be assumed as a possible reference ~~lowest boundary~~main wetting curve.

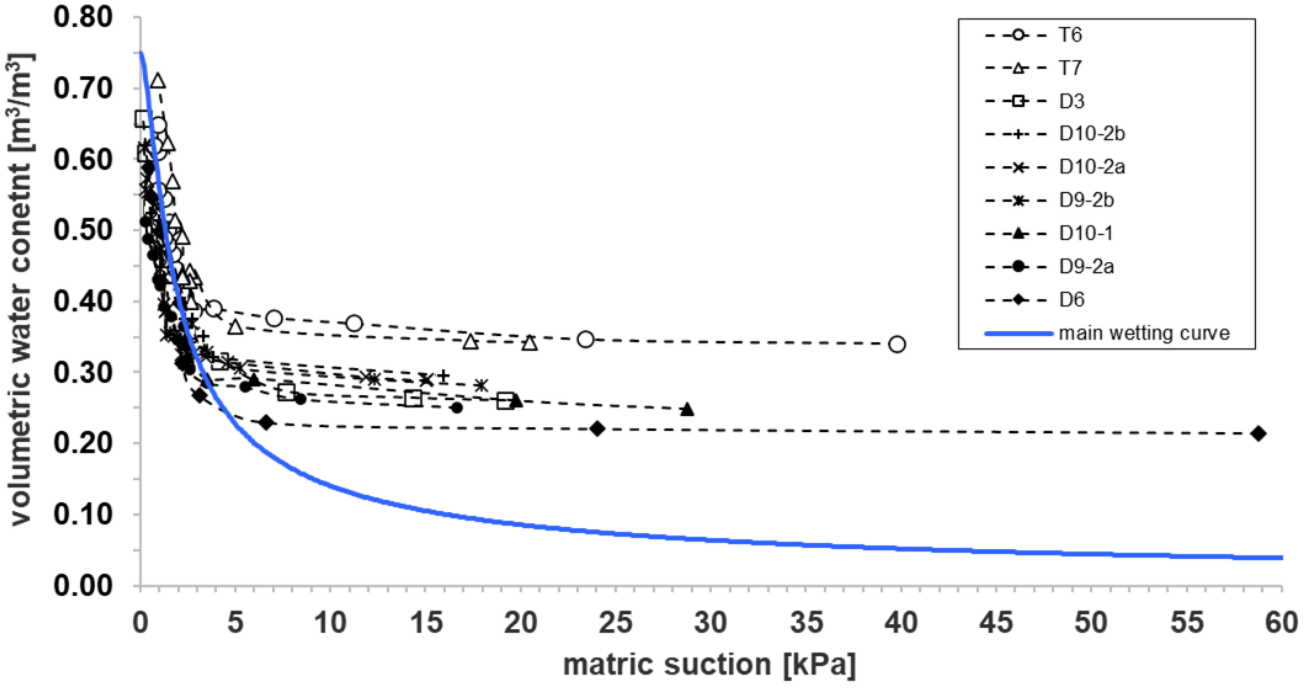

Figure ~~5~~6: Coupled values of matric suction and volumetric water content measured during infiltration tests (Damiano and Olivares, 2010~~, and Olivares et al., 2019~~). The tests acronyms shown in the legend are those reported in the repository dataset (Comegna et al., 2020).

Table 2: Van Genuchten parameters (Eq. 1), ~~representative of the~~ fitted to the ~~lowest water retention boundary~~main wetting curve shown in Figure 5~~.~~: saturated volumetric water content, θ_s; residual volumetric water content, θ_r; parameters, *α*, *n* and *m*.

ϑ_s [m^3/m^3]	ϑ_r [m^3/m^3]	α [kPa^{-1}]	*n* [-]	*m* [-]
0.75	0.00	1.00	1.72	0.42

2.3 Monitoring station

At the end of 2009, an automatic monitoring station was installed at the elevation of 560 m a.s.l., next to the right side of the landslide triggered in 1999 (Fig. 3b), to have continuous information about rainfall depth, matric suction and volumetric water content (Comegna et al. 2016a). Figure 7a shows a schematic representation of the installed devices, whose main features are reported by Table 3. Rainfall was automatically recorded at a hourly time step by a rain gauge (Fig. 7b) having a sensitivity of 0.2 mm. Suction was measured by two "Jet-fill" tensiometers, equipped with tension transducers (Fig. 7c). The 7 cm long ceramic tips of the tensiometers, named L2-1 and L2-2 (Fig. 5), were pushed into the soil, at the depths z = 0.60 m and z = 1.00 m, through small holes previously dug by a drill. The uppermost part of the hole was then filled with a bentonite–cement mixture to avoid any water infiltration. A careful maintenance was granted by regularly checking the complete saturation of the instruments (especially after long-lasting dry periods) and filling the tube with de-aired water in order to remove air bubbles. Moreover, the instruments were carefully checked during the coldest periods, featured by temperature lower than 0°C, when the de-aired water contained in the upper part of the hydraulic circuit of the tensiometers could freeze, thus affecting the correctness of the pressure transducer reading. If it occurred, we made note of that in order to give a correct interpretation of the corresponding registered data. During the cold periods we also controlled that the expanded volume of ice did not break either the pressure transducer or the plexiglass tensiometer tubes. Volumetric water content was measured by two probes for Time Domain Reflectometry (TDR), named S2-1 and S2-2 (Fig. 5), that were installed in a row with the tensiometers, at a distance of 30 cm from them. Each sensor consists of three 40 cm long metallic rods (Fig. 7d), having a diameter of 3 mm and spacing of 15 mm. The centres of S2-1 and S2-2 were respectively installed at the same depth of the ceramic tips of L2-1 and L2-2 (Fig. 5). Once vertically buried in the soil, the TDR probes were connected through coaxial cables and a multiplexer to a Campbell Scientific Inc. TDR-100 reflectometer (Fig. 7e). TDR readings provide the soil bulk dielectric permittivity, ε_r, which can be converted to θ through a calibration relationship (Topp et al., 1980). A specific relationship was purposely found by Guida et al. (2012) through targeted laboratory tests on undisturbed samples taken nearby the monitoring station; the average error in the estimation of θ is ±0.02 m^3/m^3. All the sensors were connected to the Campbell Data Logger located about 5 m far (Fig. 7e). The monitoring station was powered by a solar panel with a 12V backup battery. The automatic acquisition and storage of data was set with a time resolution of six hours.

Hourly air temperature data are also available, being provided by the Pietrastornina weather station (located at 495 m a.s.l. and 15 km from Cervinara), that is managed by the "Functional Centre for forecast, prevention and monitoring of risks and alerting for civil protection" of Campania Civil Protection Agency.

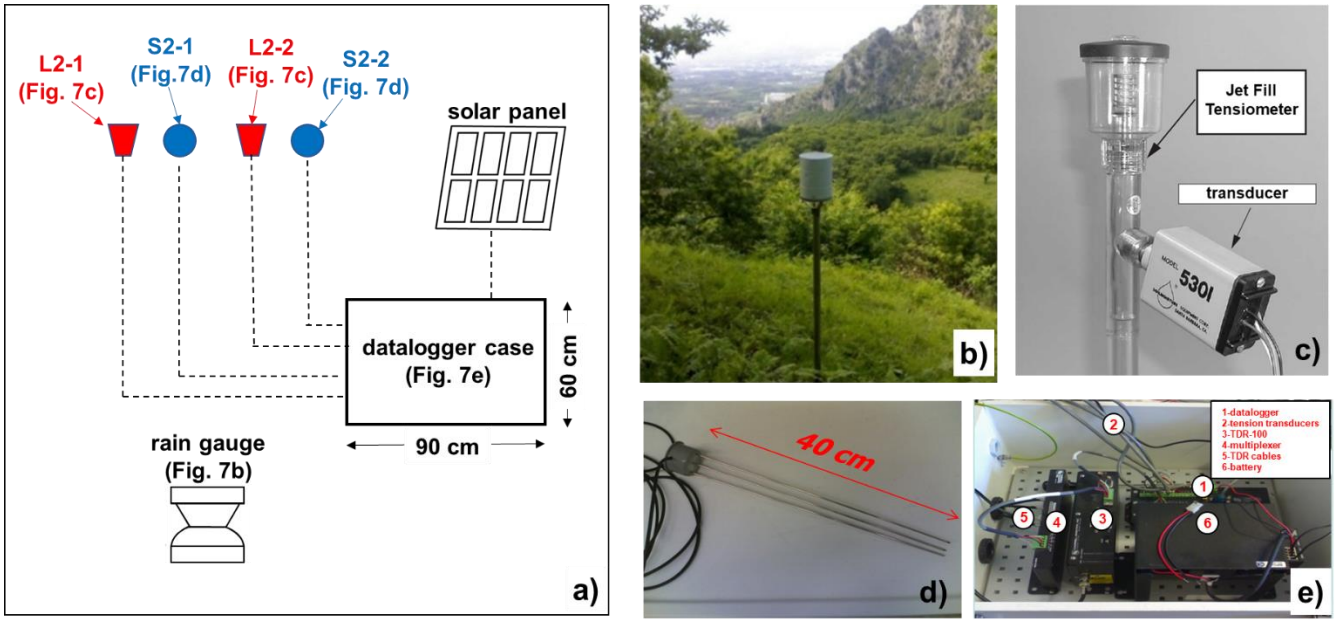

Figure 7: Installed instruments: a) schematic representation; b) rain gauge; c) "Jet-fill" tensiometer; d) TDR probe; d) datalogger case.

Table 3: Main characteristics of the installed instruments.

ELETRONIC SENSORS	*COMPANY*	*MODEL*	*MEASUREMENT RANGE*	*TEMPERATURE RANGE*	*ACCURACY*
Data logger and data Acquisition System	Campbell Scientific Inc. (Logan, UT, USA)	CR-1000	-	-25°C to +50°C	±(0.06% of reading +offset) at 0 °C to 40 °C for Analog Voltage
Time Domain Reflectometer	Campbell Scientific Inc. (Logan, UT, USA)	TDR-100	-2 m to 2100 m (distance) and 0 to 7µs (time)	-40°C to +55°C	-
Multiplexer for TDR System	Campbell Scientific Inc. (Logan, UT, USA)	SDM8 x 50	8-Channel	-40°C to +55°C	-
Tension Transducer	Soil Moisture Equipment Corp. (Goleta, CA, USA)	5301	0–85 cBar	0°C to +60°C	0.25%
Rain gauge	Campbell Scientific Inc. (Logan, UT, USA)	ARG100	0–500 mm/hr	-	-

The monitored s and θ data have been then used to carry out some analyses aimed to estimate the slope stability conditions. In particular, the factor of safety FS(z;t) at depth z and time t has been calculated by the following formula provided by the simplified infinite slope model, that is suitable for Cervinara slope (Greco et al., 2013; Comegna et al., 2016b),

$$FS(z;t) = \frac{\tan\varphi'}{\tan\alpha} + \frac{c_{app}(z;t)}{\gamma \cdot z \cdot \mathrm{sen}\alpha \cdot \cos\alpha} \quad (2),$$

where φ′ is the friction angle, α is the slope angle, γ is the unit weight of the deposit (assumed homogeneous), while c_{app}, known as *apparent cohesion*, is a strength component changing with time according to the s and θ variations. Vanapalli et al. (1996) provide the following expression for c_{app}

$$c_{app}(z;t) = s(z;t) \cdot \frac{\vartheta(z;t) - \vartheta_r}{\vartheta_s - \vartheta_r} \cdot \tan\varphi' \quad (3).$$

Therefore, c_{app}, and consequently FS, decreases with s due to infiltration. Moreover, being an assigned FS obtained by different couples of s and θ, it's possible to plot on a water retention plane different iso-FS curves, that could help to determine the current slope stability conditions.

The following Section 3 describes the field data collected from January, 1st, 2011 to January, 31st, 2012: this period has been chosen because of the abundance of data useful for a correct interpretation of the annual hydrological response.
Section 4 reports some considerations concerning the influence of the monitored hydraulic hysteresis on the slope stability conditions.

3 Results of field monitoring

~~The wetting and drying processes affecting the cover are of course strictly governed by the weather forcing, typical of the Mediterranean climate, characterized by warm and dry summer.~~ Figure ~~6~~ 8 shows the monthly cumulative precipitation~~s~~ in 2011 provided by the rain gauge installed on the slope~~, ,and the average monthly values of minimum, T_{min}, daily mean, T_{med}, and maximum, T_{max}, temperature monitored by a local weather station managed by Campania Civil Protection Agency.~~ The total cumulative rainfall was 1360 mm, a value lower than the mean yearly rainfall in the same area (Figure 4). A daily precipitation higher than 1 mm was recorded 99 times; the daily rainfall exceeded the value of 50 mm only in five cases (February, 16th; April, 30th; September, 19th; November, 6th; December, 5th). March was the rainiest month, with a total precipitation of 296 mm, i.e. 22% of the yearly rainfall. The dry season started in June continuing until the end of October. In ~~such a~~this season some significant isolated rainy events characterised by daily precipitation~~s~~ ranging between 17.4 mm and 19.2 mm occurred on July, 29th; September, 7th; October, 8th; October, 22nd; another more severe event totaling 53 mm took place on September, 19th. In the time interval November ~~and~~ December, the cumulative rainfall was about 30% of the

annual precipitation: the most intense daily rainfall occurred on November, 6th (58 mm). Figure 8 also shows the average monthly values of minimum, daily mean, and maximum temperature monitored at a hourly scale by the Pietrastornina weather station. The daily mean air temperature was close to average, with a slightly warmer summer. The potential evapotranspiration can hence be assumed to be close to the average estimated values shown in Figure 4. In particular, the mean daily temperature was higher than 15°C from May, 19th, to October, 7th, attaining values higher than 20°C from July, 30th, to September, 18th. The lowest and highest ~~T_{min}~~ average values ~~was~~ were respectively measured in February (4 °C), and ~~the highest T_{max}~~ in August (31 °C) ~~in August~~. Although some discrepancies due to the distance of the Pietrastornina weather station from the investigated slope, the temperature date above elaborated can be considered reliable.

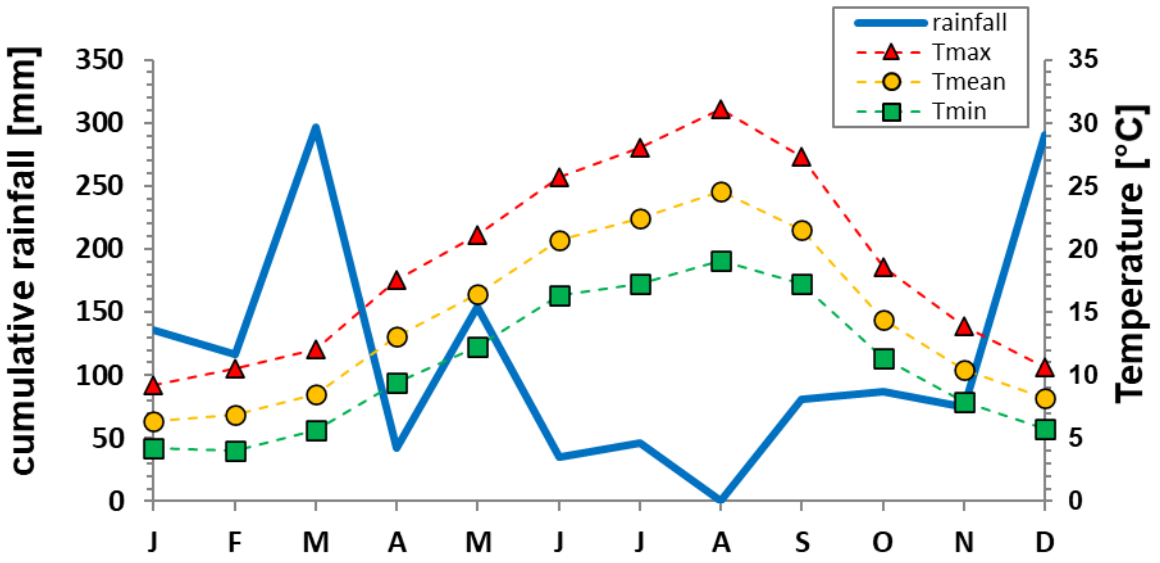

Figure ~~6~~8: Monthly cumulative rainfall and average monthly minimum (T_{min}), daily mean (~~T_{med}~~T_{mean}) and maximum (T_{max}) values of air temperature monitored in 2011.

The ~~data~~ information obtained by coupling ~~moisture content~~ θ and ~~matric suction~~ s data monitored at both the investigated depths of 0.60 m and 1.00 m are discussed in the following subsections by distinguishing eight time windows ~~characterized~~ characterised by different weather conditions. Due to some technical problems, related to the emptying of the tensiometers (occurring especially during the warmest periods) or to some loss in battery power, the records present some missing data ~~lacks~~. In particular, unfortunately no retention data are available from July, 19th to November, 4th, 2011 and from December, 6th, 2011 to January, 6th, 2012. Despite the gap, it allowed to recognize important aspects of the hysteretic hydrologic response of the investigated deposit.

3.1 Time window A-B: January, 1st - May, 8th 2011

The total precipitation in this time interval was 695 mm, which corresponds to 51% of the annual cumulative value. Until March, 12th, the mean daily air temperature ranges between 0.5°C and 12.8°C (Fig. ~~7a~~9a), then it steadily increases from 5.8°C to 16.7°C (with an increasing trend of 1.8°C/month).

On January, 1st, the ~~moisture content~~ θ and ~~matric suction~~ s values measured by S2-1 and L2-1 at depth of 0.60 m are respectively 0.39 m^3/m^3 and 11 kPa (Fig. ~~7b~~9b). ~~Such~~ These values are the result of the antecedent weather conditions; in particular, the total precipitation in the previous 30 days had been 170 mm and the mean daily air temperature 7°C (Fig. ~~7a~~9a). As shown in Figure ~~7b~~9b, the ~~soil moisture content~~ θ measured in the examined window is 0.34-0.41 m^3/m^3 while ~~the matric suction~~ s ranges in the interval 3-16 kPa. During the dry days, ~~the soil moisture~~ θ decreases with a rate of -1%/month while ~~suction~~ s tends to increase with an average rate of about 1.4 kPa/month. ~~Such a~~This drying path is periodically reversed by some rainfall-induced wetting processes. In particular, three sudden s drops ~~of suction~~ are recorded on January, 23rd, February, 17th, and May, 1st, due to very similar rainfall events featured by a total precipitation of 48-58 mm cumulated over the antecedent 48 hours.

At depth of 1.00 m, ~~the volumetric water content~~ θ, measured by S2-2, and ~~suction~~ s, measured by L2-2, range respectively in the intervals 0.29-0.37 m^3/m^3 and 4-16 kPa (Fig. ~~7c~~9c). ~~Soil moisture~~ θ tends to decrease ~~of~~ by -0.8%/month, while ~~suction~~ s is increasing with an average rate of about 1.0 kPa/month. ~~Such~~ These trends are hence slower than at the shallower depth. ~~This reflects a minor role of evapotranspiration during winter and early spring (when the vegetation is leafless), when the soil profile is slowly drained downward owing to the existing small water potential gradient, which departs from the gravitational 1 only during rainfall~~ This reflects a minor role of evapotranspiration during winter and early spring (when the vegetation is leafless). In this period, the soil profile is mainly drained downward by gravity, except during rainfall, when capillary gradient favours rapid infiltration. ~~The large amount of precipitation and t~~The small variations of ~~water content~~ θ and ~~soil suction~~ s at both depths, despite the large amount of precipitation, suggest that the soil cover is being crossed by an intense downward flux, without being retained (or being retained only in a little part) -. Rainfall events can ~~which~~ cause~~s~~ just temporary small increments of ~~water content~~ θ ~~in response to rainfall events,~~ followed by slower reductions. Indeed, at both depths ~~the water content~~ θ is steadily higher than the field capacity (i.e. about 0.25 m^3/m^3).

All data have been reported in the water retention plane s-θ, shown in Figure ~~8a~~ 10a and ~~8b~~10b, together with the corresponding manual fitting curves, named AB. At both investigated depths, the ~~fitting~~ curve AB is quite flat with an overall slope of about -0.4 %/kPa.

3.2 Time window B-C: May, 8th - June, 22nd 2011

This window is featured by a cumulative rainfall of 85 mm and a daily air temperature ranging in the interval 10-24°C, with an increasing trend of 4.3°C/month (Fig. ~~7a~~9a). During this season, vegetation starts ~~growing further and further~~ flourishing thus accommodating the increasing evapotranspiration demand and influencing the hydrological soil response through root

water uptake. The actual evapotranspiration may approach the limiting PET value, but very likely never reaching it because the atmospheric demand is not fulfilled by soil water.

At depth z = 0.60 m, ~~suction~~ s ranges between 10 kPa and 24 kPa, growing with a rate of about 9 kPa/month. This matches a θ reduction ~~in soil moisture~~, that reaches the value of 0.25 m^3/m^3 with a decreasing trend of -9 %/month (Fig. ~~7b~~9b), which is more pronounced than during the previous time window due to an intense root water uptake from the uppermost soil layer. Collected data ~~can be well~~were fitted by the curve BC in Figure ~~8a~~ 10a provided by Eq. (1) identifying the best fitting α and n parameters ~~through the parameters~~ shown in Table ~~3~~ 4 (~~using~~ assuming again θ_s = 0.75 m^3/m^3, ~~and~~ θ_r = 0, and $m = \frac{n-1}{n}$). The path BC is clearly steeper than the curve AB.

Table ~~3~~4: Van Genuchten parameters (Eq. 1) ~~representative of~~ fitted to the curve BCD ~~curve~~ shown by Figure ~~8a~~10a: saturated volumetric water content, θ_s; residual volumetric water content, θ_r; parameters, α, n and m.

ϑ_s [m^3/m^3]	ϑ_r [m^3/m^3]	α [kPa^{-1}]	n [-]	m [-]
0.75	0.00	0.11	2.17	0.54

At depth z = 1.00 m (Fig. ~~7c~~9c), until June, 6th, ~~water content~~ θ and ~~suction~~ s display little variations, moving respectively from 0.33 m^3/m^3 to 0.31 m^3/m^3 and from 15 kPa to 17 kPa. Measured values are again well fitted by the curve AB (Fig. ~~8b~~10b). After ~~such a~~this period, which is probably still ~~characterized~~ characterised by some gravitational downward drainage, the soil starts drying quickly at this depth too being forced by root water uptake. The water content decreases with a rate of about -4%/month attaining a value of 0.27 m^3/m^3 at the end of this time window, while the increasing ~~suction~~ s rate is similar to the one observed at 0.60 m. ~~Such~~ These data are well ~~interpolated~~ fitted by the path CD (Fig. ~~8b~~10b), which is steeper than the path AB, but gentler than the CD curve detected at 0.60 m because of a lower evapotranspiration effect. The fitting parameters~~,~~ are reported in Table ~~4~~5~~, are different from those obtained for z = 0.60 m (Table 3)~~. Besides to evapotranspiration effects, ~~such~~ the ~~differences~~ different responses observed at the two depths might be justified also by small differences in grain size and/or void ratio of the soil (Comegna et al., 2016a).

Table ~~4~~5: Van Genuchten parameters (Eq. 1) ~~representative of~~fitted to the curve CD shown by Figure ~~8b~~10b: saturated volumetric water content, θ_s; residual volumetric water content, θ_r; parameters, α, n and m.

ϑ_s [m^3/m^3]	ϑ_r [m^3/m^3]	α [kPa^{-1}]	n [-]	m [-]
0.75	0.00	0.76	1.33	0.25

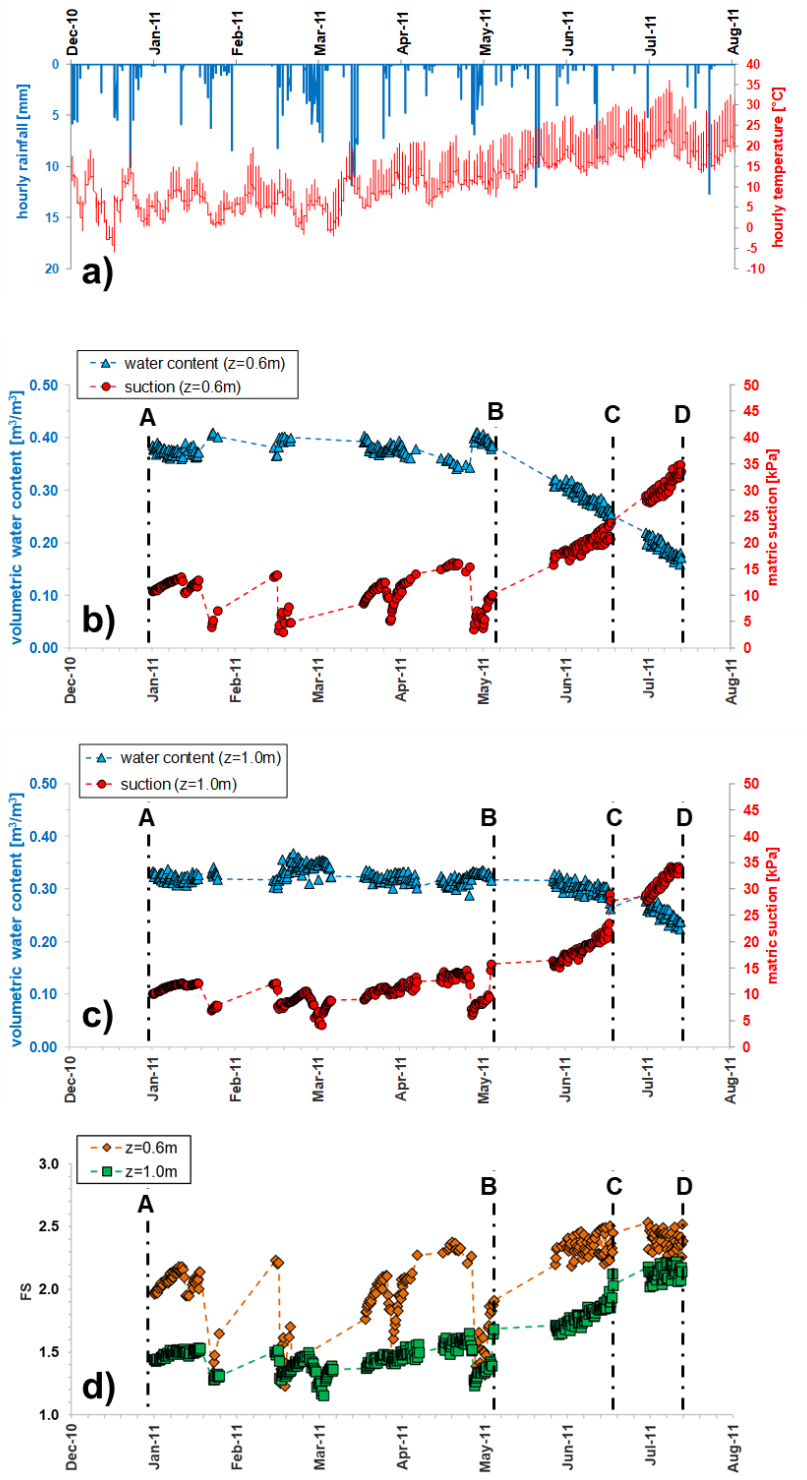

Figure ~~79~~: Hourly weather data (a), matric suction and volumetric water content monitored from January to July, 2011 at depth z = 0.60 m (b) and z = 1.00 (c), calculated factor of safety, FS (d).

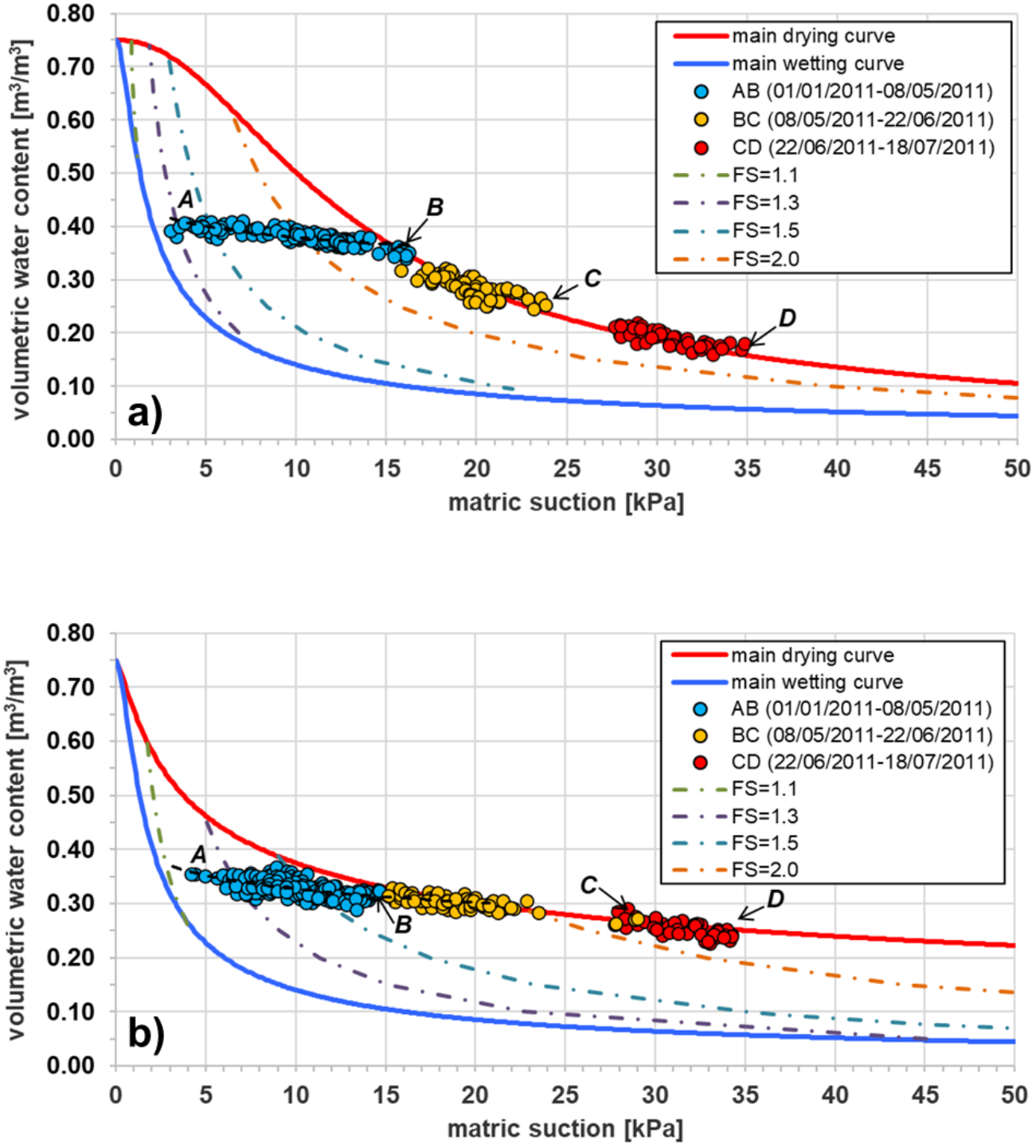

365 **Figure ~~8~~10: Volumetric water content and matric suction recorded from January to July, 2011 at depths z = 0.60 m (a) and z = 1.00 m (b) and iso-Safety Factor curves.**

3.3 Time window C-D: June, 22nd - July, 18th 2011

In ~~such a~~this dry time interval the average daily temperature is 23.7°C with an increasing trend of 3.3°C/month and the cumulative rainfall is 14 mm (Fig. ~~7a~~9a). The flourishing vegetation and the high temperature suggest that evapotranspiration ~~is~~ largely ~~exceeding~~ exceeds infiltration by rainwater, causing drainage of the soil cover ~~owing to the action of plant roots~~.

At z = 0.60 m, ~~the soil moisture~~ θ reaches a value of 0.17 m^3/m^3, while ~~suction~~ s grows by about 22 kPa/month until a value of 35 kPa (Fig. ~~7b~~9b). It is worth noting that in the retention plane the path BC can properly fit recorded field data (Fig. ~~8a~~10a). At z = 1.0 m, ~~soil moisture~~ θ reaches the value of 0.24 m^3/m^3, while ~~suction~~ s increases with a rate of about 13 kPa/month attaining a value of 34 kPa (Fig. ~~7c~~9c). In the retention plane, the field data are well interpolated by the curve CD (Fig. ~~8b~~10b).

3.4 Time window E-F: November, 5th - November, 6th 2011

In the time interval from July, 19th to November, 4th, during which, as already stated, monitoring of ~~water content~~ θ and ~~suction~~ s stops, the air temperature goes from the mean value of 24.6°C, reached in August, to 14.4°C, in October. Regarding precipitation~~s~~, from September to October the rain gauge records a cumulative precipitation of 168 mm fallen in only 9 isolated rainy days (Fig. ~~9a~~11a). Such a few concentrated precipitation~~s~~ seem to have been recorded by the shallowest sensors only. In fact, if the data acquired on November, 5th, are compared to those monitored on July, 18th, we can notice a ~~moisture~~ θ increase (from 0.17 to 0.24 m^3/m^3) and a ~~suction~~ s decrease (from 35 to 22 kPa) at 0.60 m (Fig. ~~9b~~11b), while the sensors at z = 1.00 m (Fig. ~~9c~~11c) record a small water content decrease (from 0.24 to 0.23 m^3/m^3) and a~~n~~ s increase ~~of suction~~, from 34 to 47 kPa.

The most intense daily rainfall in 2011 takes place on November, 6th. The total precipitation is 58 mm (Fig. ~~9a~~11a) and causes a ~~volumetric water content~~ θ increase from 0.24 to 0.43 m^3/m^3 (Fig. ~~9b~~11b) at 0.6 m, and from 0.23 to 0.27 m^3/m^3 at 1.0 m (Fig. ~~9c~~11c). At both depths the highest drop in ~~suction~~ s is recorded; in fact, the decrease measured by L2-1 is from 22 kPa to 1.9 kPa (Fig. ~~9b~~11b) and the one recorded by L2-2 is from 47 kPa to 13 kPa (Fig. ~~9c~~11c). These data are represented in the water retention plane by the paths EF (Figs. ~~10a~~ 12a and ~~10b~~12b) well different from those ran in May and June. It's worth noting that at the shallowest depth, the final point F reaches the curve obtained by interpolating the flume tests described in Section 2 (Fig. 5), which might be considered to be a reliable lowest boundary (the main wetting curve).

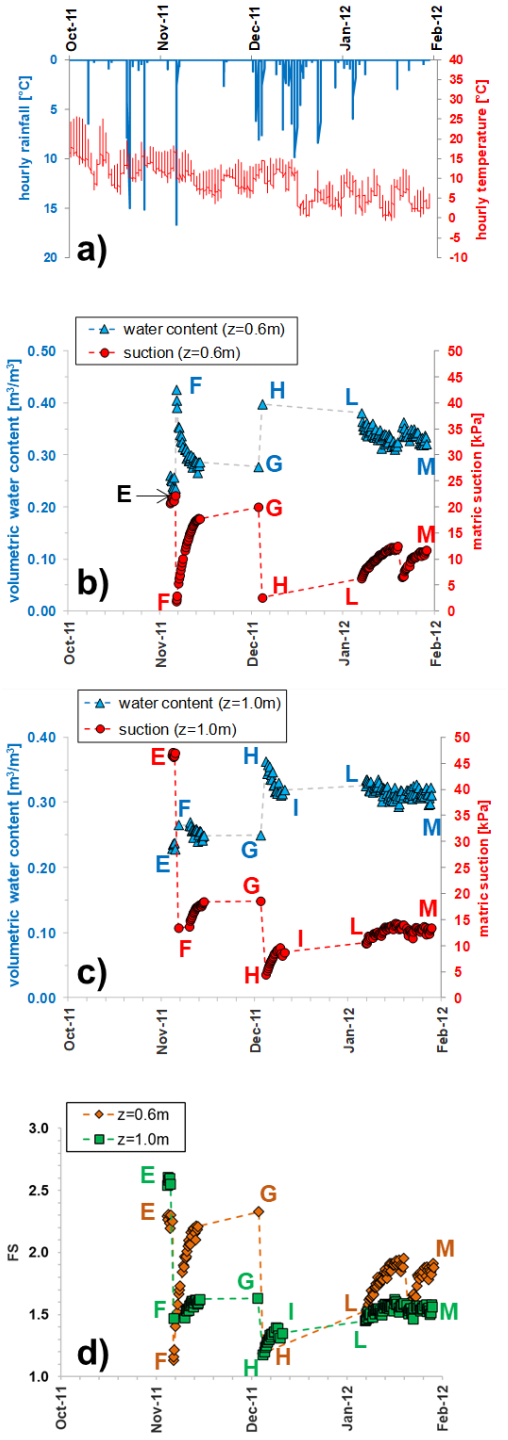

400 **Figure ~~9~~11: Monitored hourly weather data (a), matric suction and volumetric water content from November, 2011 to January, 2012 at the depth z = 0.60 m (b) and z = 1.00 (c), calculated factor of safety, FS (d).**

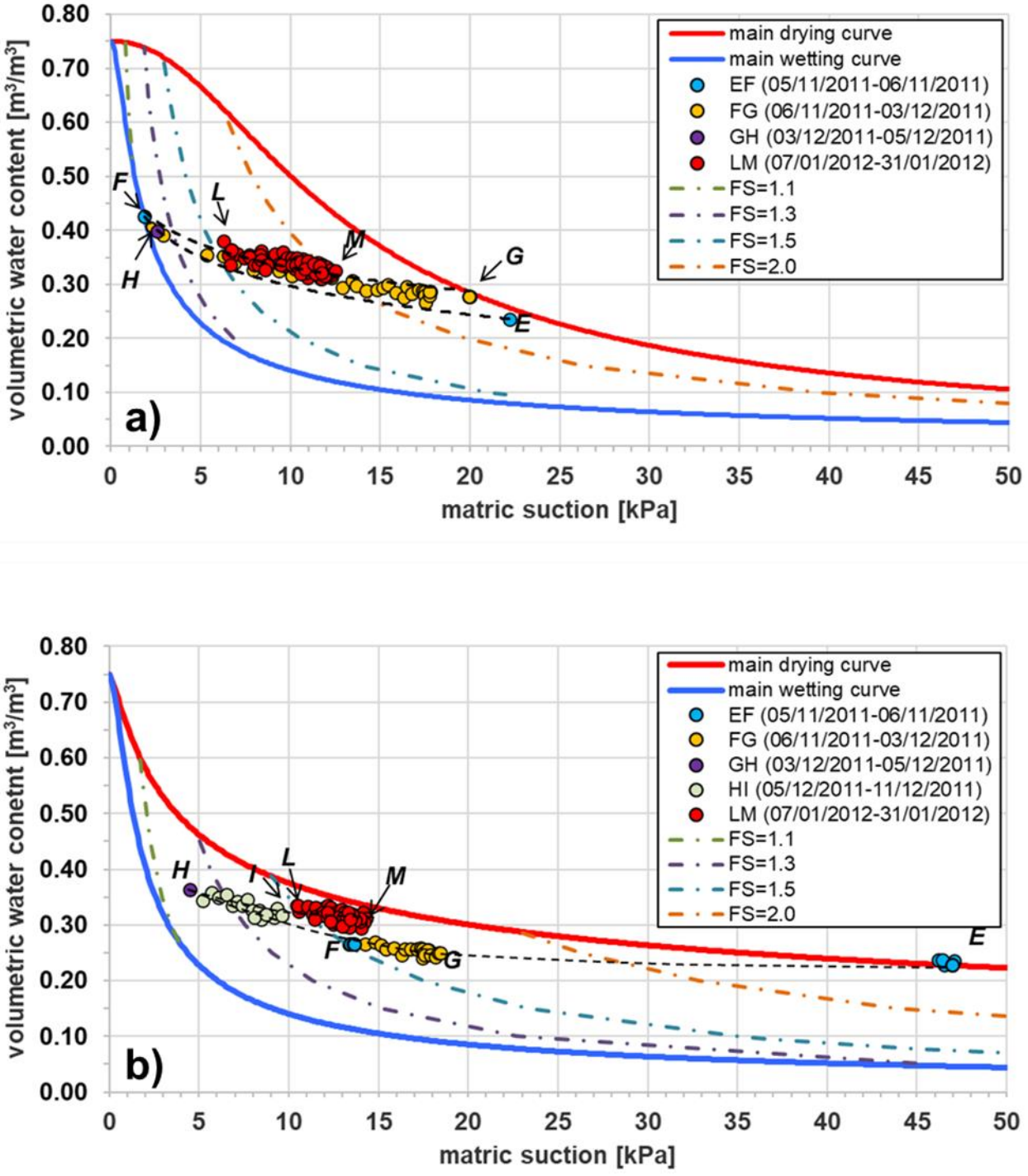

Figure ~~10~~12: Volumetric water content and matric suction, monitored from November, 2011 to January, 2012 at depths z = 0.60 m (a) and z = 1.00 m (b), and iso-Safety Factor curves.

3.5 Time window F-G: November, ~~7th~~ 6th – December, 3rd 2011

~~Such~~ This ~~a~~ time interval is ~~characterized~~ characterised by dry weather. In fact, one single rainfall event only of 12 mm occurs on November, 22nd. The mean temperature is about 10°C. During this period, when the leaves of deciduous trees fall, the vegetation enters a dormant phase, during which they need very little water. Hence, the atmospheric evapotranspiration demand, that is small as typical of winter months, is likely larger than the amount of water actually extracted from the soil by the vegetation. ~~Moreover, leafless vegetation probably did not accommodate the small evapotranspiration demand favouring an~~ An essentially downward flow, initially driven by a high potential gradient due to a wetter uppermost soil profile, is consequently favoured then progressively approaching a slow gravity driven drainage. In fact, at z = 0.60 m, ~~the water content~~ θ decreases from 0.43 to 0.28 m^3/m^3 while ~~soil suction~~ s increases from 1.9 kPa to 20 kPa (Fig. ~~9b~~11b). In the water retention plane, the corresponding drying path FG is located above previous wetting path EF, about parallel to it (Fig. ~~10a~~12a). It is worth to note that at point G it reaches the BCD curve travelled from May to July, confirming that drying develops according to smoother paths and gently approaches the field capacity (about 0.25 m^3/m^3), when soil drainage is not forced by root water uptake.

At z = 1.00 m, ~~the water content~~ θ decreases from 0.27 to 0.25 m^3/m^3 and ~~soil suction~~ s increases from 13 kPa to 19 kPa (Fig. ~~9c~~11c). The corresponding drying path FG pursues backwards previous path EF (Fig. ~~10b~~12b).

3.6 Time window G-H: December, 3rd - December, 5th 2011

On December, 5th, ~~a single~~after a precipitation of 98 mm ~~over~~ in 48 hours, ~~causes an~~ θ increases ~~of the water content~~ at both depths. ~~As a consequence~~In particular, at z = 0.60 m ~~the water content~~ θ grows from 0.28 to 0.40 m^3/m^3 and ~~suction~~ s drops to 2.5 kPa (Fig. ~~9b~~11b). The wetting curve GH overlaps previous FG drying path (Fig. ~~10a~~12a). Again, the final point H reaches the assumed lowest boundary.

At z = 1.00 m θ ~~the water content~~ increases from 0.25 to 0.36 m^3/m^3, less than above, while ~~suction~~ s decreases to 4.5 kPa. The final point H does not reach the assumed main wetting curve (Fig. ~~10b~~12b).

3.7 Time window H-I: December, ~~6th~~ 5th – December, 11th 2011

No precipitation~~s~~ occur during this short time window. Available data concern only depth z = 1.00 m. ~~The moisture content~~ θ decrease~~s~~ from 0.36 to 0.31 m^3/m^3 and ~~soil suction~~ s increases to 10 kPa (Fig. ~~9c~~11c). The drying path HI is located above and parallel to the wetting path GH (Fig. ~~10b~~12b).

3.8 Time window L-M: January, 7th, 2011 – January, 31st, 2012

~~Such a~~This period is ~~characterized~~ characterised by negligible evapotranspiration owing to cold temperatures and leafless vegetation. Hence, the observed θ and s trends ~~of water content and suction can~~ may be ascribed to gravitational downward drainage, which in the long run would lead the soil cover to approach field capacity. Until January, 21st, 2012 ~~suction~~ s increases from 6 kPa to 13 kPa at z = 0.60 m and from 10 kPa to 14 kPa at z = 1.00 m. On that date, a 12-hours cumulative 16 mm rainfall causes a drop in ~~suction~~ s of 6 kPa and 3 kPa respectively at the shallowest and deepest tensiometers. Then ~~suction~~ s increases again until the final values of 12 kPa (z = 0.60 m) and 13 kPa (z = 1.00 m) associated with ~~water contents~~ θ of 0.32 and 0.31 m^3/m^3. All field data are quite well interpolated by the paths GH at z = 0.60 m (Fig. ~~10a~~12a) and HI at z = 1.00 m (Fig. ~~10b~~12b).

4 Discussion

The ~~hydraulic~~ paths plotted in Figs. ~~8~~ 10 and ~~10~~ 12 show that, at different times, different values of ~~matric suction~~ s have been observed at both instrumented depths for the same ~~the soil moisture content~~ θ. The relationship between these two variables is then not univocal. In particular, the difference depends on the initial conditions (i.e. on the starting point). This reveals the hysteretic nature of the hydrological soil response. Therefore, all obtained paths should be considered as scanning curves located between the main drying and the main wetting curve. In more detail, the steepest drying paths obtained during the warmest days as a result of intense evapotranspiration owing to flourishing vegetation (curve BCD at z = 0.60 m; curve CD at z = 1.00 m) tend to the assumed main drying curve. It's also interesting to notice that, at 1.0 m depth, ~~such~~ this final steeper path is reached on June, 6th, i.e. with a delay of about one month with respect to the shallowest depth (where it has been attained on May, 8th). Such a result could be related to the delayed and mitigated effect of evapotranspiration due to the water uptake by roots, which are denser at depths less than 0.50 m, but are present down to a depth of 1.50 m more or less. During the periods of leafless vegetation and low temperatures, when the amount of evapotranspiration is modest, the drying paths are less steep and well below the assumed upper boundary.

According to our field data, the internal hysteresis is not particularly relevant. However, some little differences between the drying and the wetting scanning paths have been recognized at both depths when the highest θ is attained next to the main wetting curve. In particular, Figure 10a shows that the scanning path observed at depth z = 0.60 m after the rainfall event finished on November, 6th (curve FG) is above that previously monitored (curve EF); Figure 10b shows that the scanning path observed at depth z = 1.00 m after the rainfall event completed on December, 5th (curve HM) is above the one monitored before that (curve EH).

~~All wetting paths move along gentler curves than the drying paths suggesting that vegetation does not affect soil wetting.~~

For the sake of clarity, it has to be pointed out the tensiometers and the TDR probes sample different soil volumes; this might lead to an imperfect matching of data, i.e. any variation in s and in θ is not simultaneously detected by the sensors. For

instance, if the wetting front advances downward, the 40 cm long TDR probe can detect it with some advance compared to the ceramic tip of the tensiometers (the centres of the two sensors are aligned, so the upper edge of the TDR probe is above the upper edge of the tip). The temporal mismatch will be larger for steeper wetting front. A similar issue would affect the edges of the sensors during vertical (gravity-driven) drainage processes, while soil drying caused by root uptake is expected to be more evenly distributed throughout the entire root zone. These issues would certainly affect the coupling especially in the initial stage of infiltration and drainage process, which are characterized by steeper gradients. However, the measurements are acquired every six hours, and looking at Figures 9 and 11, it appears that s and θ variations at the two investigated depths, 40 cm apart from each other, are detected nearly simultaneously. Hence, it is expected that the temporal mismatch may affect only one or two measurement points during each of the wetting/drying paths discussed in Figures 10 and 11, which consist of many measurement points as they refer to long lasting processes.

In order to estimate to what extent the slope stability conditions are affected by ~~such a~~the hysteretic response, some simple analyses have been carried out by the infinite slope model ~~that is a suitable for Cervinara slope (Greco et al., 2013; Comegna et al., 2016b)~~. In particular, the factor of safety FS at depth z has been calculated by Eq. (2) assuming a homogeneous deposit with slope angle α = 40°, unit weight γ = 14 kN/m^3, cohesion c' = 0, friction angle φ' = 38°, ~~saturated volumetric water content~~ θ_s = 0.75 m^3/m^3, ~~residual water content~~ θ_r = 0~~,~~. ~~the factor of safety FS at depth z is provided by the formula:~~.

~~$$FS = \frac{\tan\varphi'}{\tan\alpha} + \frac{c_{app}}{\gamma \cdot z \cdot \mathrm{sen}\alpha \cdot \cos\alpha} \qquad (2)$$~~

~~where $c_{app} = s \cdot \frac{\vartheta - \vartheta_r}{\vartheta_s - \vartheta_r} \cdot \tan\varphi'$ is the expression provided by Vanapalli et al. (1996) to define the *apparent cohesion*, a strength component which accounts for the role of suction. Assuming, γ constant for the sake of simplicity, t~~ the variation of FS with time is only due to ~~c_{app}~~ fluctuations of the apparent cohesion, c_{app}. In particular, being φ' lower than α, FS remains higher than one only if c_{app} is higher than a threshold value that could be calculated by Eq. (2). Regarding the examined case, ~~In particular, Eq. (2) shows that,~~ at depths z = 0.60 m and z = 1.00 m, slope stability is guaranteed respectively by ~~an apparent cohesion equal to or higher than~~ c_{app} ≥ 0.3 kPa~~,~~ and ~~and by~~ c_{app} ≥~~=~~ 0.5 kPa ~~or more at z = 1.00 m~~.

Figures ~~11~~ 9d and ~~12~~ 11d show the fluctuations of ~~the safety factor~~ FS during the period of monitoring. At z = 0.60 m, FS ranges between a minimum value of 1.13, attained on November, 6th (Fig. ~~12a~~11d), and a maximum of 2.22, on July, 5th (Fig. ~~11a~~9d), which respectively correspond to c_{app} values of 0.8 and 6.6 kPa. At z = 1.00 m, FS ranges between 1.18 and 2.60, on December, 5th, and on November, 5th (Fig. ~~12b~~11d), corresponding to a c_{app} interval 1.5-11.6 kPa. The higher fluctuation of FS at the shallowest depth, z = 0.60 m is obviously due to a higher ~~suction~~ s variation.

In Figures ~~8~~ 10 and ~~10~~ 12 the iso-Safety Factor curves, i.e. featured by constant FS values, have been plotted. ~~At~~ For a given ~~suction, s~~, FS increases with ~~the soil moisture;~~ θ. this means that the lower scanning curves correspond to worse safety conditions. For instance, looking at Figure ~~10~~12, the FS values calculated along the wetting path EF, that originates after the dry season, are lower than those corresponding to the drying curve LM that starts after the rainfall events occurred in

November and in December; also, the changing rate of ~~the safety factor~~ FS is always remarkable along the scanning paths where little θ changes ~~of the soil moisture content~~ can induce high ~~suction~~ s changes.

It is interesting to notice that the lowest FS value is attained at z = 0.60 m on November, 6th, i.e. after the most intense rainfall event recorded in 2011, when the wetting path reaches the assumed lower boundary at point F (Fig. ~~10a~~12a), featured by s = 1.9 kPa and θ = 0.43 m^3/m^3. Starting from this condition, a further, just hypothetical, persistent and intense rainfall event could have forced the point to follow the final steeper branch of the main wetting curve~~, which has been obtained the flume tests (Fig. 5)~~. In particular, the failure condition (FS = 1) would have been reached for ~~a soil moisture~~ θ = 0.69 m^3/m^3 (s = 0.40 kPa), i.e. for an ~~water content~~ increase $\Delta\theta$ = 0.26 m^3/m^3 (or a ~~suction~~ decrease Δs = -1.5 kPa). Such a large increase in the water content indicates that landsliding in the area at hand is not so obvious, being the consequence of exceptional weather conditions as chronicles and statistical analyses suggest (Comegna et al., 2017).

5 Conclusions

The setup of an automatic field station allowed monitoring the annual cyclic hydrological response of a sloping deposit in pyroclastic air-fall soils. Even though the relationship between measured volumetric water content~~s~~ and suction values has to be carefully considered accounting for all the factors which can adversely affect ~~the~~ its validity ~~of such a relationship~~ (small differences in grain size or porosity, which is dependent also on the installation procedures of the sensors into the soil ~~around the sensors~~, different soil volumes affecting the response of sensors, different reliability in data interpretation), monitoring provide~~d~~ useful information about the hydrological soil response.

In particular, collected data highlight the influence of the initial conditions, which depend on the antecedent wetting/drying history, on the weather-induced hydraulic paths. In fact, different ~~soil moisture~~volumetric water contents ~~values~~ can be associated with the same matric suction due to the hysteretic soil response. Moreover, soil drying may be affected by evapotranspiration due to water ~~exctraction~~ extraction by roots, ~~and this in a different way~~ which varies throughout ~~in~~ the ~~different~~ seasons.

As indicated by simple stability analyses, in the examined period the slope has been ~~always quite~~ far from failure conditions. In particular, the hydraulic path leading to slope failure ~~is~~ should have ~~generally~~ featured by quite ~~a~~ high ~~soil moisture~~volumetric water content change~~s~~. This ~~is~~ are well detectable by TDR sensors, but ~~is~~ are ~~characterized~~ characterised by so low suction changes (less than 2 kPa) to be hardly measurable by ordinary tensiometers. ~~Such~~ These results unavoidably raise some questions on the best way to set up reliable early warning systems in areas threatened by rapid landslides in shallow unsaturated granular soil covers. These systems should be indeed based on: i) a monitoring system able to provide real time updates about the weather-induced hydraulic paths, and ii) a forecasting model accounting for the soil water retention properties. Both should be supported by the knowledge of the main drying and wetting curves that bound the water retention domain.

~~The research is continuing in order to check the validity and repetitiveness of collected data and to deepen the soil response to weather forcing.~~

Data availability

The datasets, ~~are~~ freely downloadable from https://doi.org/10.5281/zenodo.4281166 (Comegna et al., 2020~~).~~), are provided through the following five separate Excel files:

- 1_Field data_ rainfall, containing the hourly rainfall measured in the considered time period (January, 1st, 2011 – January, 31st, 2012) by the rain gauge;
- 2_Field data_ temperature, containing the hourly temperature measured in the considered time period (January, 1st, 2011 – January, 31st, 2012) by the weather station located in the town of Pietrastornina and managed by the regional Civil Protection Agency;
- 3_Field data_suction & moisture content_z=0.6m, containing s and θ measured in the considered time period (January, 1st, 2011 – January, 31st, 2012) at the depth z = 0.60 m respectively by tensiometer L2-1 and TDR probe S2-1 at a time resolution of 6 hours;
- 4_Field data_suction & moisture content_z=1.0m, containing s and θ measured in the considered time period (January, 1st, 2011 – January, 31st, 2012) at the depth z = 0.60 m respectively by tensiometer L2-2 and TDR probe S2-2 at a time resolution of 6 hours;
- 5_Flume infiltration tests, containing the s and θ measured during nine flume tests induced by an artificial rainwater infiltration, carried out by Damiano and Olivares (2010).

Author contribution

LC, ED, RG and LO installed the automatic monitoring station and took care about the maintenance of the instruments. LC analysed the monitored field data. ED and LO analysed the results of the laboratory infiltration tests to assume a reliable main wetting curve. LC and LP jointly conceived and set up the paper, discussing the issues with the other three authors. RG provided considerations about the role of vegetation. The contributions of the authors are equal.

Competing interests

The authors declare that they have no conflict of interest.

Acknowledgements

The "Functional Centre for forecast, prevention and monitoring of risks and alerting for civil protection" of Campania Civil Protection Agency is gratefully acknowledged for providing temperature data.

References

Chen, P., Mirus, B., Ning, L., and Godt, J.W.: Effect of Hydraulic Hysteresis on Stability of Infinite Slopes under Steady Infiltration, Journal of Geotechnical and Geoenvironmental Engineering, 143(9), doi:10.1061/(ASCE)GT.1943-5606.0001724, 2017.

Chen, P., Ning, L, and Wei, C.: General Scanning Hysteresis Model for Soil–Water Retention Curves, Journal of Geotechnical and Geoenvironmental Engineering, 145(12), doi:10.1061/(ASCE)GT.1943-5606.0002184, 2019.

Comegna, L., Damiano, E., Greco, R., Guida A., Olivares, L., and Picarelli, L.: Effects of the vegetation on the hydrological behavior of a loose pyroclastic deposit, Procedia Environmental Sciences, 19, 922-931, doi:10.1016/j.proenv.2013.06.102, 2013.

Comegna, L., Damiano, E., Greco, R., Guida A., Olivares, L., and Picarelli, L.: Field hydrological monitoring of a sloping shallow pyroclastic deposit, Canadian Geotechnical Journal, 53(7), 1125-1137, doi:10.1139/cgj-2015-0344, 2016a.

Comegna, L., Damiano, E., Greco, R., Guida A., Olivares, L., and Picarelli, L.: Considerations on the Cervinara slope failure, Landslides and Engineered Slopes - Experience, Theory and Practice, vol. 2, 663-670, doi:10.1201/9781315375007, 2016b.

Comegna, L., Damiano, E., Greco, R., Olivares, L., and Picarelli, L.: Coupled monitoring of soil moisture and suction in pyroclastic air-fall silty soils, Zenodo, doi:10.5281/zenodo.4281166, 2020.

Comegna, L., De Falco, M., Jalayer, F., Picarelli, L., and Santo A.: The role of the precipitation history on landslide triggering in unsaturated pyroclastic soils, Advancing Culture of Living with Landslides, vol. 4, 307-313, doi: 10.1007/978-3-319-53485-5_35, 2017.

Comegna, L., Rianna, G., Lee, S., and Picarelli, L.: Influence of the wetting path on the mechanical response of shallow unsaturated sloping covers, Computers & Geotechnics, 73(3), 164–169, doi:10.1016/j.compgeo.2015.11.026, 2016c.

Damiano, E.: Meccanismi di innesco di colate di fango in terreni piroclastici, PhD Thesis, Università di Roma La Sapienza, 2004.

Damiano, E., and Olivares, L.: The role of infiltration processes in steep slope stability of pyroclastic granular soils: laboratory and numerical investigation, Natural Hazards, 52, 329-350, 2010.

Damiano, E., Olivares, L., and Picarelli L.: Steep-slope monitoring in unsaturated pyroclastic soils, Engineering Geology, 137-138, 1-12, 2012.

Fiorillo, F., Guadagno, F.M., Aquino, S., and De Blasio, A.: The December 1999 Cervinara landslides: further debris flows in the pyroclastic deposits of Campania (southern Italy), Bulletin of Engineering Geology and the Environment, 60(3), 171–184, doi:10.1007/s100640000093, 2001.

Greco, R., Comegna, L., Damiano, E., Guida, A., Olivares, L. and Picarelli L.: Hydrological modelling of a slope covered with shallow pyroclastic deposits from field monitoring data, Hydrol Earth Syst Sci, 17, 4001–4013, doi:10.5194/hess-17-4001-2013, 2013.

Guadagno, F.M., Revellino, P., and Grelle, G.: The 1998 Sarno landslides: conflicting interpretations of a natural event, Proceedings of the 5th International Conference on Debris-Flow Hazards Mitigation: Mechanics, Prediction and Assessment, Italian Journal of Engineering Geology and Environment, Casa Editrice Universita La Sapienza, url: www.ijege.uniroma1.it. doi:10.4408/IJEGE.2011-03.B-009, 2011.

Guida, A., Comegna, L., Damiano, E., Greco, R., Olivares, L., and Picarelli, L: Soil characterization from monitoring over steep slopes in layered granular volcanic deposits, Proceedings of the 2nd Italian Workshop on Landslides, Naples, 28–30 September 2011, Edited by L. Picarelli, R. Greco, and G. Urciuoli, Cooperativa Universitaria Editrice Studi, Fisciano, 147–153, 2012.

Li, XS: Modelling of hysteresis response for arbitrary wetting/drying paths, Computers and Geotechnics, 32, 133-137, 2005.

Marino, P., Comegna, L., Damiano, E., Olivares, L., and Greco, R.: Monitoring the hydrological balance of a landslide-prone slope covered by pyroclastic deposits over limestone fractured bedrock, Water, 2020 (submitted for publication).

Mualem, Y.: Hysteretical models for prediction of the hydraulic conductivity of unsaturated porous media, Water Resour Res, 12, 1248-1254, 1976.

~~Olivares, L., Andreozzi, L., Damiano, E., Avolio, B., and Picarelli, L.: Hydrologic response of a steep slope in unsaturated pyroclastic soils, Proceedings of the International Conference on Fast Slope Movements – Prediction and Prevention for Risk Mitigation, Naples, 11–13 May 2003, Edited by L. Picarelli, Patron Editore, Bologna, Vol. 1, 391–398, 2003.~~

~~Olivares, L., Damiano, E., Netti, N., and de Cristofaro, M.: Geotechnical Properties of Two Pyroclastic Deposits Involved in Catastrophic Flowslides for Implementation in Early Warning Systems, Geosciences, 9(1), 24, doi:10.3390/geosciences9010024, 2019.~~

~~Olivares, L., and Picarelli, L.: Shallow flowslides triggered by intense rainfalls on natural slopes covered by loose unsaturated pyroclastic soils, Geotechnique, 53(2), 283–288, 2003.~~

Pham, H.Q.: An engineering model of hysteresis for soil–water characteristic curves, MSc thesis University of Saskatchewan, Canada, 2002.

~~Picarelli, L., Evangelista, A., Rolandi, G., Paone, A., Nicotera, M.V., Olivares, L., Scotto di Santolo, A., Lampitiello, S., and Rolandi, M.: Mechanical properties of pyroclastic soils in Campania Region, Proceedings of the 2nd International Work. on Characterisation and Engineering Properties of Natural Soils, Singapore, Vol. 3, 2331–2383, 2006.~~

Pirone, M., Papa, R., Nicotera, M.V., and Urciuoli, G.: Evaluation of the hydraulic hysteresis of unsaturated pyroclastic soils by in situ measurements, Procedia Earth and Planetary Sciences, 9, 163-170, 2014.

Rianna, G., Comegna, L., Pagano, L., Picarelli, L., and Reder, A.: The role of hydraulic hysteresis on the hydrological response of pyroclastic silty covers, Water, 11(3), 628, doi:10.3390/w11030628, 2019.

Tami, D., Rahardjo, H., and Leong, E.C.: Effects of hysteresis on steady-state infiltration in unsaturated slopes, J Geotech Geoenviron Eng, 130(9), 956-966, 2004.

Tarantino, A.: A water retention model for deformable soils, Géotechnique, 59(9), 751-762, 2009.

Thornthwaite, C.W.: An approach toward a rational classification of climate, Transactions of the American Geophysical Union, 27(1), 1946.

Topp, G.C., Davis J.L., and Annan A.P.: Electromagnetic determination of soil water content: measurement in coaxial transmission lines, Water Resour. Res., 16, 574-582, 1980.

van Genuchten, M.T.: A closed-form equation for predicting the hydraulic conductivity of unsaturated soils, Soil Sci. Soc. Am. J., 44, 892-898, 1980.

Vanapalli, S.K., Fredlund, D.G., Pufahl, D.E., and Clifton AW.: Model for the prediction of shear strength with respect to soil suction, Canadian Geotechnical Journal, 33, 379-392, 1996.

Wheeler, S.J., Sharma, R.S., and Buisson, M.S.R.: Coupling of hydraulic hysteresis and stress–strain behaviour in unsaturated soils, Géotechnique, 53(1), 41-54, 2003.

Yang, C., Sheng, D., and Carter, J.P.: Effect of hydraulic hysteresis on seepage analysis for unsaturated soils, Computers and Geotechnics, 41, 36-56, 2012.